Chirality-driven delocalization in disordered waveguide-coupled quantum arrays

Gleb Fedorovich,[1,2,*] Danil Kornovan,[1] Alexander Poddubny,[3] and Mihail Petrov[1]
[1]*ITMO University, Birzhevaya Liniya 14, 199034 Saint Petersburg, Russia*
[2]*Department of Physics, ETH Zurich, Zurich 8093, Switzerland*
[3]*Rehovot 7630567, Israel*

(Received 14 July 2021; revised 8 October 2022; accepted 10 October 2022; published 28 October 2022)

We study theoretically the competition between directional asymmetric coupling and disorder in a one-dimensional array of quantum emitters chirally coupled through a waveguide mode. Our calculation reveals a highly nontrivial phase diagram for the eigenstates' spatial profile, nonmonotonously depending on the disorder and directionality strength. The increase of the coupling asymmetry drives the transition from Anderson localization in the bulk through delocalized states to chirality-induced localization at the array edge. Counterintuitively, this transition is not smeared by strong disorder but becomes sharper instead. Our findings could be important for the rapidly developing field of waveguide quantum electrodynamics, where chiral interactions and disorder play crucial roles.

DOI: 10.1103/PhysRevA.106.043723

I. INTRODUCTION

Localization of waves and particles in disordered media remains one of the key universal concepts in modern physics [1] starting from the first theoretical prediction by Anderson [2]. One-dimensional (1D) systems are especially remarkable since, according to the classical scaling theory [3], all of the states are localized for an arbitrarily weak disorder. However, the situation changes drastically in non-Hermitian disordered quantum systems, where one can observe both localized and delocalized states [4–8]. In this regard, one of the most interesting platforms is offered by waveguide quantum electrodynamics [9,10], studying interactions of localized quantum emitters with photons propagating in a one-dimensional waveguide. Such a system is inherently strongly non-Hermitian due to the presence of radiative losses and also features long-range light-induced couplings, that have recently been predicted to suppress localization [11]. Photon-photon interactions driven by anharmonicity of the emitter Hamiltonians can enable quantum chaos [12], and many-body localization [13]. The effects of disorder have been also extensively studied in an alternative non-Hermitian system based on semiconductor polaritonic lattices [14–16] and complex systems with loss and gain [17].

The situation becomes even more interesting in the regime of chiral quantum optics [18], when a constant magnetic field applied transverse to the waveguide introduces artificial "chirality" to the system and makes light-induced couplings between the atoms partially unidirectional [see Fig. 1(a)]. The directional coupling appears due to polarization dependent waveguide mode excitation. This destroys the internal symmetry of the problem and also suppresses the quantum interference effects responsible for localization. However, despite recent numerical studies of the photon transmission and reflection through chiral disordered atomic arrays [19–21] and the recent interest in non-Hermitian skin effects [22–24], as well as scaling theory of localization in chiral non-Hermitian systems [25], the fundamental problem of localization in non-Hermitian disordered systems with directional couplings is still open.

Here, we study theoretically localization and delocalization of a single excitation in an array of atoms with fluctuating frequencies, depending on the fluctuation strength and the directionality of the atom-waveguide mode coupling. We reveal a delicate competition between the chirality and disorder strength. The origin of the competition is straightforward: disorder tends to localize the states in the bulk area, while chirality tends to localize the states at the edge of the system. We show that, counterintuitively, the effect of a chiral coupling is not universal and it can either localize or delocalize eigenstates depending on the disorder strength, as is schematically illustrated in Fig. 1(b). The advantage of the considered atomic chiral setup is its high coherence and tunability by external magnetic field [26]. However, our theoretical results are quite general and apply both to quantum and classical chiral systems. For example, topological photonic structures [27], where the unidirectional propagation of protected edge states is one of the central scenarios, attract now a lot of interest [28–30].

II. THEORETICAL FRAMEWORK

A. General description of a chiral disordered array

We start with the consideration of a 1D array of N two-level quantum emitters placed at the coordinates $z_n \equiv nd$, $n = 1, 2 \ldots$, and coupled through a single guided mode, which is schematically shown in Fig. 1(a). In the case of a finite system, the effective Hamiltonian can be represented as $\widehat{H} = \widehat{H}_0 + \widehat{V}$

*gleb.fedorovich@metalab.ifmo.ru

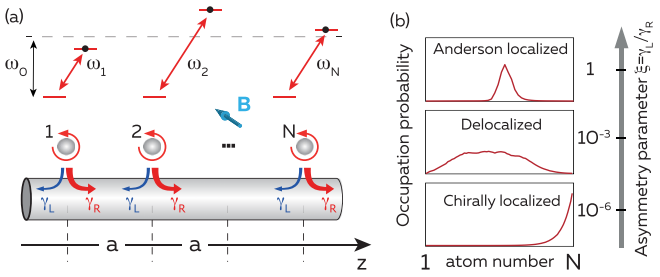

FIG. 1. (a) The geometry of an array of regularly spaced quantum emitters separated by a distance a and directionally coupled through a waveguiding mode. (b) Localized and delocalized eigenstates depending on the coupling directionality parameter $\xi \equiv \gamma_L/\gamma_R$ calculated for $\delta = 0.05$ and $N = 100$, having the eigenfrequencies $(\omega - \omega_0)/\gamma_0 = 0.48, 0.03,$ and 0.01, respectively.

with [31]

$$\widehat{H}_0 = \hbar \sum_{m=1}^{N} \left(\omega_m - i\frac{\gamma_0}{2}\right)\widehat{\sigma}_m^+ \widehat{\sigma}_m^-, \quad \widehat{V} = \hbar \sum_{\substack{m,n=1 \\ m\neq n}}^{N} g_{n,m}\widehat{\sigma}_n^+ \widehat{\sigma}_m^-, \tag{1}$$

where $\omega_m \equiv \omega_0 + \Delta\omega_m$ and γ_m are the transition frequency and radiative emission rate of the mth emitter, respectively, and $g_{n,m}$ are the emitter-emitter coupling constants. We focus on the diagonal disorder due to the fluctuations of transition frequencies of the mth emitter so that the fluctuations $\Delta\omega_m$ are normally distributed random numbers with standard deviation equal to $\delta\gamma_0$ in the absence of correlations between the emitters. The radiative emission rates are assumed to be constant for all emitters, $\gamma_m = \gamma_0$. The proposed theoretical model can potentially find an experimental realization, for instance, in a cold-atomic array localized in the vicinity of a nanofiber in a periodic optical potential [32] with random fluctuations or a nanofiber with corrugated surfaces. The fluctuating stable atom-fiber distance will provide random Lamb shift in the energy of atomic transitions. Alternatively, one may suggest a superconducting circuit [33] with random inharmonicity, which will also contribute to random fluctuations of the transition energy of artificial atoms.

The interemitter coupling constants $g_{n,m}$ can be expressed through the electromagnetic Green's function [31,34]. They depend on the polarization properties of both the guided mode and the transition dipole moments, and take the form $g_{n,m} = -i\gamma_R e^{i\varphi_{nm}}$ for $m > n$, and $g_{n,m} = -i\gamma_L e^{i\varphi_{nm}}$ for $m < n$, where $\gamma_R = \gamma_0/(1+\xi)$ and $\gamma_L = \xi\gamma_R$ are emission rates to the right and left directions, correspondingly, and parameter $\varphi_{nm} = k_0|z_n - z_m|$ is the phase due to propagation of a photon between the emitters n and m. The parameter $\xi, 0 \leqslant \xi \leqslant 1$, characterizes the degree of asymmetry.

Here, we focus on singly excited quasistationary states of the emitter array $|\psi_m\rangle = \sum_{n=1}^{N} c_{nm}\sigma_n^+|0\rangle$, which are collective polaritonic states formed due to the long-range coupling of emitters through the guided mode [35–38]. Their eigenfrequencies Ω_k in a finite structure are complex valued due to the radiative decay rate, and can be found from the following Schrödinger equation:

$$\widehat{H}\,|\psi_m\rangle = \hbar\Omega_m\,|\psi_m\rangle\,, \quad \Omega_m = \omega_m - i\gamma_m/2. \tag{2}$$

More details on the eigenstates of regular infinite and finite periodic structures are provided in Appendices A and B, respectively. The following analysis of the effects of disorder relies on the properties of eigenfunctions $|\psi_m\rangle$ of the equation above. However, the localization effects can also be manifested in the optical response of the system, for example, the transmission coefficient, and the next subsection will cover this aspect.

B. Localization length estimated from the transmission spectra

Another subject we want to cover in this section is how to extract the localization length from the transmission coefficient through the structure.

In principle, propagation and localization of waves in one-dimensional disordered structures should be described by a general phase formalism [39] that has been successfully applied to photonic structures; see Ref. [40] and references therein. However, generalization of the phase formalism for the case of directional coupling is a separate task that lies out of the scope of the current paper. Instead, we resort here to a more simplified semiphenomenological approach that ignores interference of waves reflected from different atoms but still captures the essence of light localization away from the resonance frequency ω_0. Specifically, the reflection coefficient of light from the mth atom can be presented as

$$r_m = \frac{\sqrt{\gamma_L\gamma_R}}{\omega_m - \omega - i\gamma_0/2} \approx \langle r\rangle + \delta r_m, \tag{3}$$

$$\langle r\rangle = \frac{\sqrt{\gamma_L\gamma_R}}{\omega_0 - \omega - i\gamma_0/2}, \tag{4}$$

$$\delta r_m = -\frac{\sqrt{\gamma_L\gamma_R}}{(\omega_0 - \omega - i\gamma_0/2)^2}\delta\omega_m, \tag{5}$$

where $\delta\omega_m \equiv \omega_m - \omega_0$ is the frequency fluctuation, $\gamma_R = \gamma_0/(1+\xi)$, and $\gamma_L = \xi\gamma_R$. Here, $\langle r\rangle$ is the coherent part of the reflection coefficient, responsible for the formation of the polaritonic band gap in the ordered structure. On the other hand, δr_m is the disorder-induced reflection, zero on average, but responsible for wave localization. In writing Eq. (3) we have assumed that the frequency is far enough from atomic resonance so that it is sufficient to take into account only one term in the Taylor expansion in powers of frequency fluctuations $\delta\omega_m$. Our next crucial simplification, assuming strong uncorrelated disorder, is the independent transmission of waves through different atoms, without taking into account multiple reflections:

$$T_N = T_{N-1}\left(1 - \left|\delta r_N^2\right|\right). \tag{6}$$

Equation (6) indicates that the probability of the wave to pass through N atoms is given by the probability of light to pass through $N-1$ atoms times the probability of not being scattered by the disorder at the Nth atom. We stress that Eq. (6) does not take into account the coherent part of the reflection coefficient $\langle r\rangle$ that does not contribute to wave localization away from the band gap and just renormalizes the wave dispersion law.

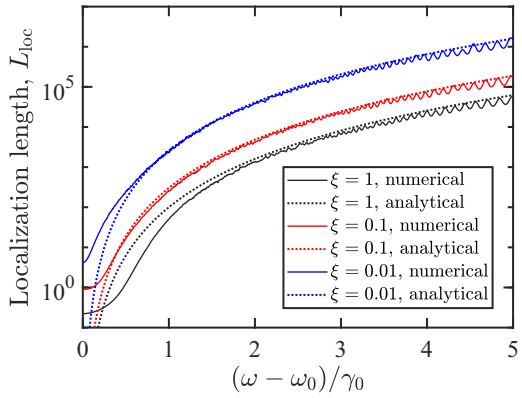

FIG. 2. Frequency dependence of the localization length calculated numerically from Eq. (7) and analytically from Eq. (9) for three different values of the directionality parameter ξ, fixed disorder strength $\delta = 0.2\gamma_0$, and period that implies $\phi_{n,n+1} = k_0\Delta z = \pi/2$. The array length was chosen to be $N = 1000$, and the averaging has been done over 500 disorder realizations.

Given that $\langle \delta r_N^2 \rangle \ll 1$ we find from Eq. (6) the decay law for the transmission coefficient

$$\ln T_N \propto -\frac{N}{L_{\rm loc}}, \tag{7}$$

$$\frac{1}{L_{\rm loc}} = \langle |\delta r_m|^2 \rangle, \tag{8}$$

where $L_{\rm loc}$ is the length of extinction (being equivalent to the localization length in the case of a one-dimensional system) and the angular brackets denote averaging over the disorder. Calculating the average $\langle |\delta r_m|^2 \rangle$ we obtain the formula that estimates $L_{\rm loc}$ provided that $|\omega - \omega_0| \gg \gamma_0$:

$$L_{\rm loc}(\omega, \xi) = \frac{(1+\xi)^2(\omega - \omega_0)^4}{\xi \gamma_0^4 \delta^2}. \tag{9}$$

A more formal equivalent derivation of Eq. (9) for the localization length in case of symmetric coupling, $\xi = 1$, based on the phase formalism and the Fokker-Planck equation is presented in Ref. [40].

As this equation is only a rough analytical estimate of the localization length, one also needs to calculate a precise numerical value of the transmission coefficient, which can be done using the transfer-matrix approach, which is widely known, and theoretical details of which are covered in Appendix C.

Figure 2 presents the comparison of the localization length, calculated numerically by averaging the logarithm of the transmission coefficient over the disorder, following Eq. (7), and analytically, following Eq. (9). The analytical and numerical results are in a good quantitative agreement, especially in an expected region $\omega - \omega \gg \gamma_0$ far enough from the band gap. By this we confirm the qualitative validity of Eq. (9), which we will use in the next section when discussing the results.

III. NUMERICAL RESULTS AND DISCUSSIONS

We characterize the spectrum of a finite disordered structure with the density-of-states (DOS) function. The spatial distribution of the eigenstates is described by the participation ratio parameter (R) [41], that quantifies the effective number of the occupied sites by a single excitation, and reads $R_m = (\sum_{i=1}^N |c_{im}|^2)^2 / \sum_{i=1}^N |c_{im}|^4$ for the mth state. Since the polaritonic eigenmodes of the ordered periodic array are just the delocalized Bloch waves, the excitation occupies almost all of the lattice sites and $R \sim N$. On the other hand, for a localized eigenstate we expect smaller values of $R \approx 1$, independent of N.

The DOS profiles shown in Fig. 3(a) have a typical two-peak structure that can be understood from the polariton dispersion in a periodic array described in Appendix A. The DOS manifests a band gap around the frequency ω_0 resulting from the avoided crossing of the light line with the atomic resonance [10]. The band-gap width is equal to γ_0 in case of $\varphi = \pi/2, \xi = 1$[36]; see also Fig. 6. The DOS function has van Hove singularities at the gap edges typical for one-dimensional systems. As expected, disorder leads to the smearing of the band edges, and formation of the Urbach tails [41], where the states are strongly localized as can be seen from Fig. 3(b). With the increase of the asymmetry (smaller ξ) the polaritonic band gap gets more narrow as can be directly seen from the comparison of Figs. 3(a) and 3(b) with Figs. 3(c) and 3(d). For small asymmetry parameters the band-gap width becomes comparable to the energy of Urbach tails, and there appears nonzero density of states in the band-gap center with a relatively small value of R in Fig. 3(d). In the symmetric case $\xi = 1$, localization length $L_{\rm loc}$ increases fast when the frequency is detuned from the atomic resonance. For $|\omega - \omega_0| \equiv |\Delta\omega| \gg \gamma_{L,R}$ the localization length can be approximately estimated from the expression we derived in the previous section: $L_{\rm loc}(\omega, \xi) = (1+\xi)^2(\omega - \omega_0)^4/\xi\gamma_0^4\delta^2$. In order to distinguish between the localized and extended eigenstates for a finite array it is instructive to compare the localization length with the array size, $L_{\rm loc}(\omega, \xi) = N$, because if the array is shorter than the localization length then the eigenstate is spread over all atoms. The obtained frequency dependence $L_{\rm loc}(\omega, \xi)$ is shown by the black dashed curve in Fig. 3(e). It is in qualitative agreement with the numerical solution of $L_{\rm loc}(\omega, \xi) = N$ where the localization length has been extracted from the disorder-averaged logarithm of the numerically calculated transmission coefficient through a finite array as $1/L_{\rm loc} = -\langle \ln |t_N^2| \rangle / N$ (solid curve). Specifically, for $\xi = 1$ the central spectral region in Figs. 3(a), 3(b), and 3(e) with frequencies $|\Delta\omega/\gamma_0| \lesssim 0.4$ corresponds to the band gap with no eigenstates [white color in Fig. 3(e)], and it is surrounded by a region of Anderson-localized states with $0.4 \lesssim |\Delta\omega/\gamma_0| \lesssim 0.7$ (blue color). For even larger detunings $\Delta\omega$ the localization length exceeds the array size and the states become extended [red color in Fig. 3(e)].

The profile of eigenstates changes dramatically for an asymmetric array with $\xi < 1$. The effect of coupling asymmetry is twofold. First, the smaller the ξ the narrower the spectral region of localized states and the narrower the band gap in the ordered structure [see black curves in Fig. 3(e)]. This is the consequence of the suppression of back reflections and Anderson localization in the strongly chiral setup with $\xi \ll 1$.

Strong asymmetry of the interaction destroys both the polaritonic bands and Anderson localization in the bulk of the system. However, one can consider an extreme case of

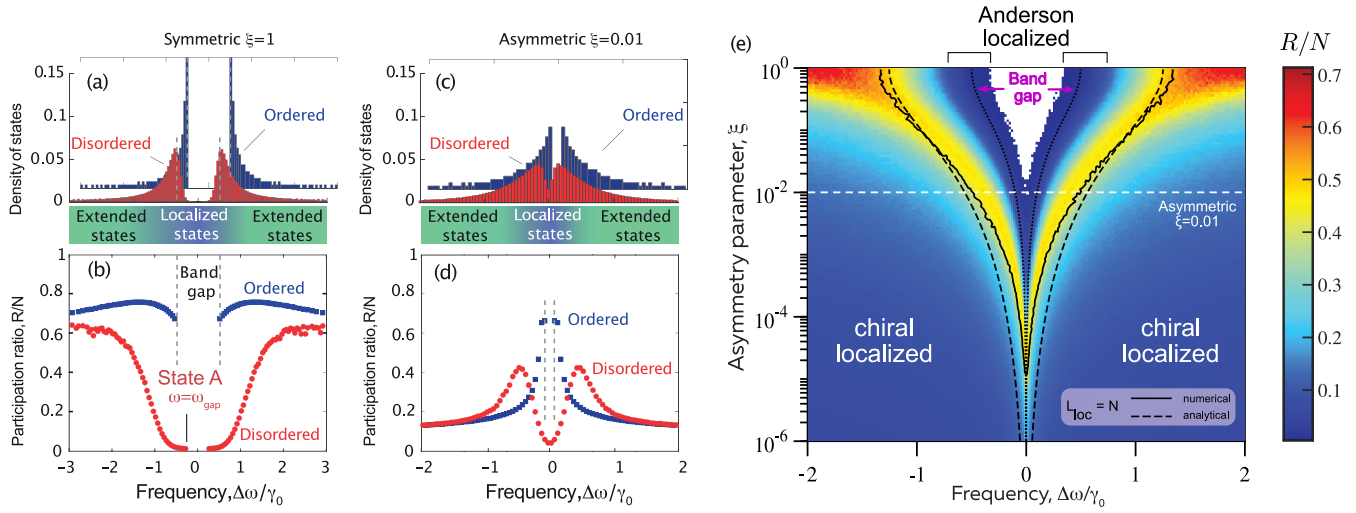

FIG. 3. (a)–(d) Density of states (a), (c) and normalized participation ratios R/N (b), (d) for the ordered ($\delta = 0$, blue color) and disordered ($\delta = 0.1$, red color) system with symmetric atom-waveguide coupling (a), (b) and directional (c), (d) coupling with $\xi = 0.01$. (e) Normalized participation ratio of eigenstates for a fixed disorder amplitude $\delta = 0.1$ as a function of the frequency detuning $\Delta\omega$ and asymmetry parameter ξ. Blue and red regions correspond to localized and delocalized states, respectively. The dotted black curve illustrates the band gap in an ordered array, that closes for smaller ξ. Solid and dashed black curves show the boundary between localized and extended states $L_{\rm loc} = N$, where the localization length $L_{\rm loc}$ is calculated numerically and analytically. The horizontal dashed line indicates the value $\xi = 0.01$ corresponding to panels (c), (d). The simulation parameters for (a)–(d) are $N = 400$ and $\varphi = \pi/2$; for (e) they are $\delta = 0.1$, $N = 1000$. The results were obtained after averaging over 1000, for (a)–(d), and 100, for (e), random realizations.

$\xi \to 0$, when all of the states are squeezed to the right edge of the system due to chiral localization [outer blue region in Fig. 3(e) that corresponds to the chiral localization]. Such a chiral localization can be also seen as a direct manifestation of a so-called non-Hermitian skin effect [23,24]. Indeed, for small ξ all of the modes are almost completely degenerate with $\Omega_k = \omega_0 - i\gamma_0/2$ and are strongly localized at the right edge of the chain even in the absence of disorder. This is explained by the fact that each emitter radiates to the left weaker than to the right in the asymmetric coupling case. In the limit $\xi \to 0$ only one nontrivial state survives, $|N\rangle \equiv \sigma_N^+|0\rangle$, and it is localized at only a single atom at the edge of the chain (see Appendix D for details). When disorder is introduced the spectral degeneracy is lifted and N nondegenerate eigenmodes become smeared over a few sites close to the edge of the system (see Fig. 9 in Appendix D) with inverse localization length $1/L_{\rm loc}$ having a logarithmic dependence on the disorder amplitude as can be seen from Fig. 9. In order to obtain this

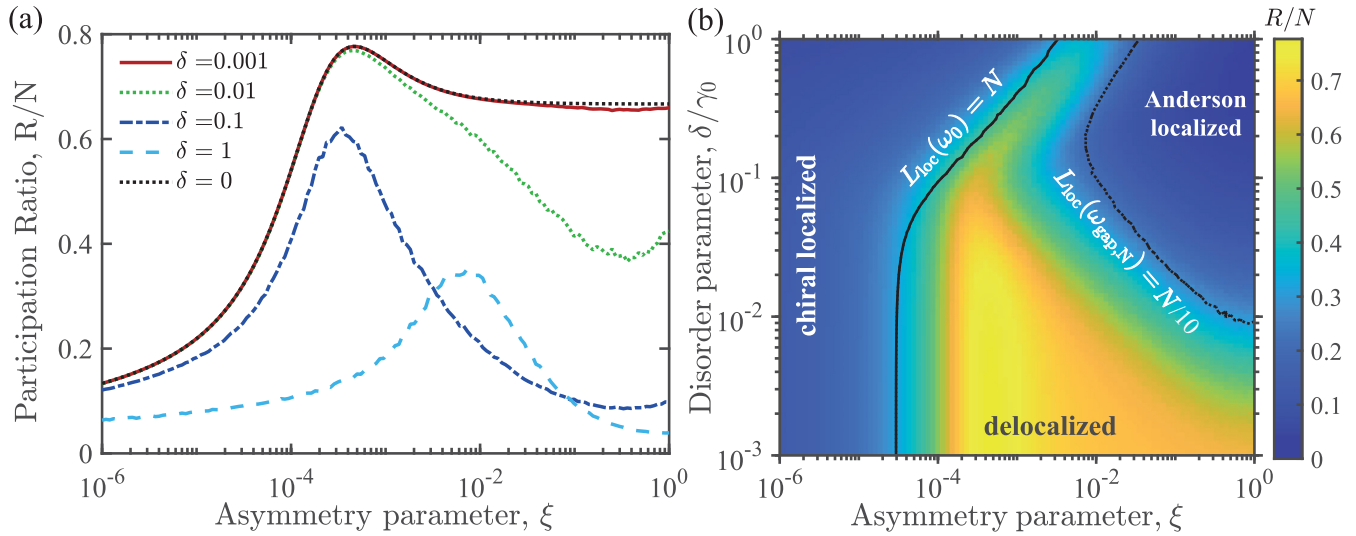

FIG. 4. (a) Normalized participation ratio for the state A closest to the resonance [see Fig. 3(a)] calculated depending on the asymmetry parameter ξ for several disorder strengths δ. (b) False color map of the participation ratio for the state A ($\omega_{\rm gap}$) depending on both ξ and δ. Black solid and dashed curves have been extracted from disorder-averaged localization length defined through a transmittance; the details are explained in the text. The number of random realizations used for averaging in (a) and (b) is 500; calculation has been performed for $N = 100$ emitters.

figure, we pick the state with the largest R for each realization of disorder, average it over multiple realizations, and fit it with the exponential function for the atoms close to the right edge of the chain.

Finally, the most striking effect is observed in the transition region for a moderate value of the asymmetry parameter ξ. In this case, for a fixed spectral detuning, e.g., $\Delta\omega = 0.5\gamma_0$, the diagram in Fig. 3(e) indicates the appearance of delocalization (at $\xi \approx 0.1$, marked with a dashed white line) on the way of gradual transition from Anderson disorder-induced localization ($\xi \to 1$) to a chiral localization ($\xi \to 0$). Appearance of the region with a large participation number indicates that chirality suppresses the effect of disorder and states become extended at the scale of the array size. Since the results in Fig. 3(e) have been obtained after averaging the R of states in a finite energy range, the contributions from localized and delocalized states could potentially be mixed and affect the average R. In order to verify that this is not the case, it is instructive to follow directly the evolution of individual eigenstates with the increase of asymmetry, which has been done in Fig. 4. Specifically, for each disorder realization we select one eigenstate that is spectrally closest to the resonance frequency ω_0; see label A in Fig. 3(b). Next, we focus on this state and analyze in Fig. 4 the transition from symmetric to chiral coupling for different values of the disorder amplitude δ. Figure 4(b) shows the dependence of the R on both δ and ξ and Fig. 4(a) presents the slices of this dependence for several characteristic disorder strength values δ. The calculation demonstrates that for the symmetric case and small disorder, the eigenstate extends over the whole system. With the increase of disorder amplitude δ, the closest to band-gap center state occupies a small part of the array and $R/N \lesssim 0.1$, which is a sign of Anderson localization in the bulk of the system.

For an extremely strong asymmetry ($\xi \to 0$) the state naturally becomes localized at the edge of the system due to the directional interaction. The boundary of this localized-states region can be estimated from $L_{\mathrm{loc}}(\omega_0, \xi) = N$ with localization length evaluated numerically from the transmission coefficient through a finite array at the transition frequency, which also corresponds to the closure of the band gap due to disorder. The corresponding boundary, extracted from the extinction spectra, is shown by a black curve in Fig. 4(b) and agrees well with the result of the calculation of the participation ratio. However, for moderate values of asymmetry parameter $\xi \gtrsim 10^{-4}$ and relatively weak disorder $\delta \lesssim 0.1$, there exists a transition region, shown by yellow colors in Fig. 4(b), where the states are extended, and occupy a significant part of the array. In this transition region the interaction asymmetry leading to edge localization competes with the disorder, which tries to localize the state in the bulk of the system. Thus, if we fix disorder strength, the transition from the Anderson localization at $\xi = 1$ to a chiral edge localization at $\xi \to 0$ is indeed nonmonotonous, and occurs through extended states. Counterintuitively, when the disorder strength increases from $\delta = 10^{-3}$ to 0.1, this transition becomes sharper and shifts, i.e., it occurs in a narrower range of a parameter ξ and for smaller values of ξ. For an even stronger disorder, $\delta > 0.1$, the values of ξ corresponding to the transition begin to increase. The second (right)

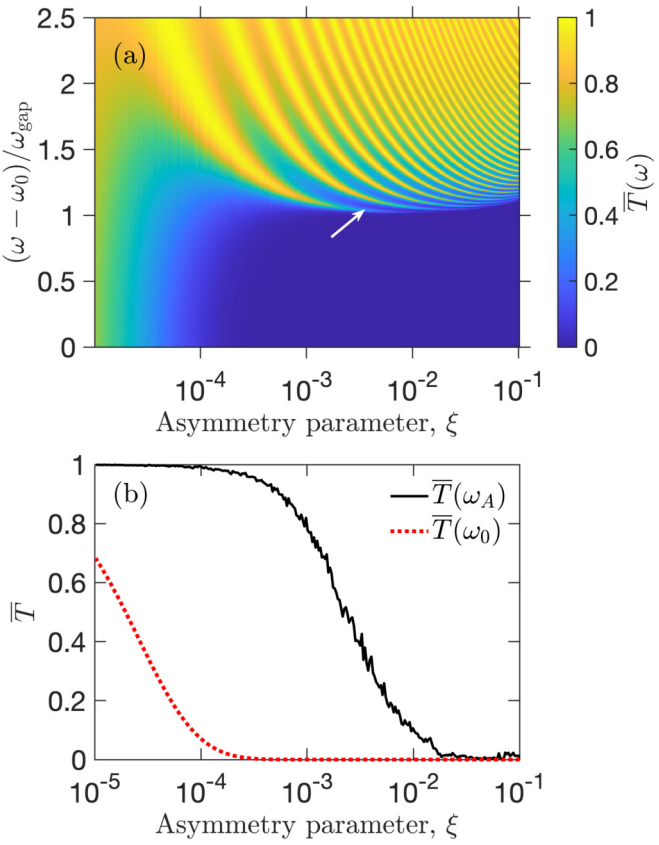

FIG. 5. (a) Dependence of the transmission spectra on the asymmetry parameter ξ. Calculated for a disorder parameter $\delta = 10^{-2}$. (b) Transmission coefficient calculated at the resonance frequency and at the frequency of the closest to atomic resonance ω_0 peak, shown by an arrow in the panel (a).

boundary between the Anderson localization and delocalization can be qualitatively found if one equates the localization length [defined through transmittance $T(\omega)$] at the frequency of the state closest to the band gap for absent disorder in a finite system to, for example, 10% of the system size: $L_{\mathrm{loc}}(\omega_{\mathrm{gap},N}) = N/10$. In case of Fig. 4(b) this second boundary is shown in dashed black, and it separates the states that are Anderson localized due to disorder from the yellow transition region. Characteristic disorder-localized, extended, and chiral-localized eigenstates are also shown in Fig. 1(b).

The transition from Anderson localization to delocalization to chiral localization can be directly detected in the transmission spectrum. To this end we have plotted in Fig. 5(a) the disorder-averaged transmission spectra $\overline{T} \equiv \exp[\langle \ln T \rangle]$ for a fixed disorder strength δ. The averaging of transmission logarithm $\langle \ln T \rangle$ has been performed over $N_{\mathrm{av}} = 60$ disorder realizations. The frequency axis has been normalized to the gap half width in the ordered system ω_{gap}.

The transmission peaks correspond to the eigenmodes of the finite array and the phase diagram Fig. 4(b) can be reproduced by tracing the peak dependence on the asymmetry and disorder parameters. In order to illustrate this, we plot in Fig. 5(b) the asymmetry dependence of the transmission coefficient at the resonance, $\overline{T}(\omega_0)$, and the transmission at the frequency of the eigenstate closest to the gap center, $\overline{T}(\omega_A)$,

shown by an arrow in panel (a). Three qualitatively different ranges of the asymmetry parameter can be distinguished. For $\xi \gtrsim 10^{-2}$ the transmission is suppressed both at the ω_A frequency and at the resonance frequency. This corresponds to the regime of Anderson localization. In the intermediate range, $10^{-4} \lesssim \xi \lesssim 10^{-2}$, the transmission coefficient $\overline{T}(\omega_A)$ starts to increase [solid black curve in Fig. 5(b)]. This reflects quenching of disorder and delocalization of the corresponding eigenstate. Finally, when the asymmetry becomes even stronger, $\xi \lesssim 10^{-4}$, the transmission coefficient $\overline{T}(\omega_0)$ also becomes large [dotted red curve in Fig. 5(b)]. This means that the whole array becomes transparent and backscattering is suppressed even at the resonance. Thus, the structure is in the fully chiral regime (when all eigenstates are localized due to strong interaction asymmetry). An analysis of such transmission maps for different values of disorder strength δ has allowed us to obtain the black curves $L_{\text{loc}}(\xi) \equiv -1/\langle \ln T \rangle$ in Fig. 3(b) and, thus, to independently reproduce the phase diagram previously found from the study of the spatial profile of the eigenstates.

Taking into account disorder in the radiative emission rate of each atom γ_n will provide "nondiagonal" disorder [42] which may enable new intriguing effects in the system such as Dyson singularity [43–45]. At the same time, introducing correlated disorder [46] will make the disorder contribution in the chirality-disorder competition more pronounced but keeping the physical picture the same.

IV. SUMMARY

To summarize, we have considered a periodic one-dimensional array of two-level emitters with disorder in transition frequencies that are asymmetrically coupled through a waveguide mode and have revealed a delicate competition between the conventional Anderson localization and the chiral localization. As a result, at moderate values of asymmetry parameter the chirality suppresses the localization, which leads to the transition from bulk localized states to edge localized states via extended states.

We believe that our findings will be important for a rapidly developing field of waveguide QED, where chiral interactions and disorder play a critical role. The modern experimental setups and platforms such as fiber-coupled cold atoms [26,47] and superconducting circuits [48] have been already used for observing chiral interactions in complex quantum systems. The estimated and experimentally reported range of asymmetry parameter $10^{-3} < \xi < 10^{-1}$ [26,47–50] enables observation of the predicted delocalization effects in realistic systems. Moreover, the extension of the obtained results to the multiphoton domain will be of significant interest due to a tremendous progress of theoretical [51–53] and experimental studies in this area [33,54] as well as generalization of our approach to nonstationary Floquet-type systems [17,55–57].

ACKNOWLEDGMENTS

The authors are thankful to Ivan Iorsh and Vladimir Yudson for fruitful discussions. Numerical and analytical calculations using the transmission coefficient performed by G.F., D.K., and M.P., were funded by Russian Science Foundation (RSF) Grant No. 21-72-10107, and calculations involving eigenstates performed by D.K. were funded by RSF Grant No. 21-72-00096. M.P. also acknowledges support by the Priority 2030 Federal Academic Leadership Program, and also from the Foundation for the Advancement of Theoretical Physics and Mathematics BASIS.

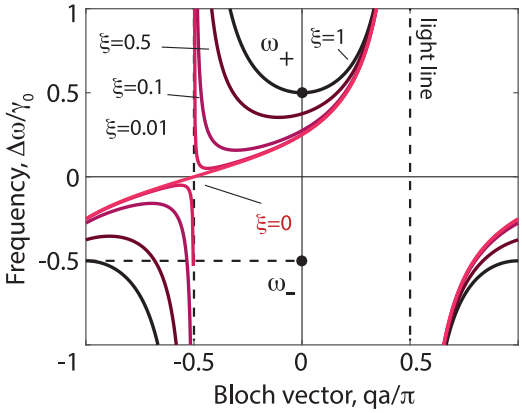

FIG. 6. The dispersion of polaritonic modes in a regular array with account for chiral interactions shown for different values of asymmetry parameter ξ.

APPENDIX A: DISPERSION OF AN INFINITE PERIODIC CHAIN

In this section, we derive the dispersion relation for an infinite ordered chain with an arbitrary coupling directionality ξ. Namely, starting from the ansatz for the eigenstate wave function $|\varphi\rangle = \sum_{n=-\infty}^{+\infty} e^{iqan} |n\rangle$ (where the $|n\rangle$ state corresponds to the nth emitter being excited, while all the others are in the ground state) and substituting into the equation

$$\widehat{H}|\varphi\rangle = \widehat{H_0}|\varphi\rangle + \widehat{V}|\varphi\rangle = \hbar\Big(\omega - i\frac{\gamma_0}{2}\Big)\sum_{n=-\infty}^{+\infty} e^{iqan}|n\rangle + \hbar \sum_{n,m=-\infty}^{+\infty} g_{m,n}\widehat{\sigma}_n^{+}\widehat{\sigma}_m^{-} \sum_{n'=-\infty}^{+\infty} e^{iqan'}|n'\rangle = E|\varphi\rangle\,, \tag{A1}$$

one can obtain the following dispersion relation:

$$\Delta\omega(q) = \frac{\gamma_0}{2(1+\xi)}\left[\cot\left(\frac{\varphi - qa}{2}\right) + \xi\cot\left(\frac{\varphi + qa}{2}\right)\right], \tag{A2}$$

which can also be found in Ref. [58].

The dispersion curves calculated for three characteristic values of the parameter ξ are shown in Fig. 6. The change of the asymmetry parameter from $\xi = 1$ to 0 makes the dispersion nonreciprocal, $\Delta\omega(q) \neq \Delta\omega(-q)$. It also leads to the closure of the band gap, as described by the equation

$$E_g = \omega_+ - \omega_- = \frac{2\sqrt{\xi}}{1+\xi}\gamma_0.$$

APPENDIX B: FINITE REGULAR CHAIN

Once the system becomes finite, the nonzero radiative losses appear due to photon escape at the edge of the array, and the eigenfrequencies of the collective states acquire the imaginary parts following Eq. (2). The wave functions of the eigenstates $|\psi_k\rangle = \sum_n c_{nk}\,|n\rangle$ can be found analytically both for symmetric and asymmetric coupling by generalizing the results of Ref. [59]:

$$c_k = e^{iq_+(k-N-1)} + r_{\hookleftarrow} e^{iq_-(k-N-1)} \propto r_{\hookrightarrow} e^{iq_+ k} + e^{iq_- k}. \quad \text{(B1)}$$

Here, the wave vectors $q_\pm$ satisfy the dispersion equation Eq. (A2) at the eigenmode frequency Ω and are chosen in such a way that $\mathrm{Im}\, q_+ > 0$, $\mathrm{Im}\, q_- < 0$. The representation Eq. (B1) shows that the eigenmode of a finite array is given by a superposition of corresponding forward- and backward-propagating Bloch waves of the infinite system. The Bloch waves transform into each other due to the reflection at the internal left and right boundaries of the array with the corresponding reflection coefficients:

$$r_{\hookrightarrow} = -\frac{1-e^{i(\varphi-q_+)}}{1-e^{i(\varphi-q_-)}}, \quad r_{\hookleftarrow} = -\frac{1-e^{i(q_-+\varphi)}}{1-e^{i(q_++\varphi)}}. \quad \text{(B2)}$$

The two representations in Eq. (B1) are equivalent to each other because the following identity holds at the eigenmode frequency:

$$r_{\hookleftarrow}(\Omega) r_{\hookrightarrow}(\Omega) e^{i(q_+-q_-)(N+1)} = 1. \quad \text{(B3)}$$

Equation (B3) is a closed-form equation that can be used to find the eigenfrequencies Ω. It has the same physical meaning as the Fabry-Pérot condition for the eigenmodes of a planar cavity. The only difference is that the problem is now discrete, and instead of just forward and backward going photons we consider polaritonic waves. In practice, however, Eq. (B3) is not easier to solve than the linear eigenproblem Eq. (2).

We now discuss these eigenmodes in more details in specific cases of symmetric and asymmetric coupling.

1. Symmetric coupling

In the case of symmetric coupling the eigenfrequencies form a circular structure [36] in the complex plane typical for Toeplitz-type matrices [60]. In order to plot the dispersion of a finite system, one can map the obtained eigenfrequencies of collective states to the first Brillouin zone of an infinite structure.

The eigenfrequencies for an array of $N = 100$ emitters and the phase parameter $\varphi = \pi/2$ are plotted in Fig. 7 for (a) symmetric $\xi = 1$ and (b) asymmetric $\xi = 10^{-4}$ coupling. They form a discrete set of points on the dispersion line of the infinite system (gray solid line in Fig. 7). The color of points in the figure denotes the radiative decay rates for each particular state, clearly showing that the states close to the band edge have the smallest decay rate (subradiant), while the states close to the avoided crossing region possess the strongest radiative losses due to the better phase matching with the waveguide mode. In the insets, we plot the distribution of wave-function amplitudes $|c_{nk}|^2$.

The radiative losses of subradiant and superradiant states scale with the size of the system as $\gamma_{\mathrm{sub}} \propto N^{-3}$ [61,62], while

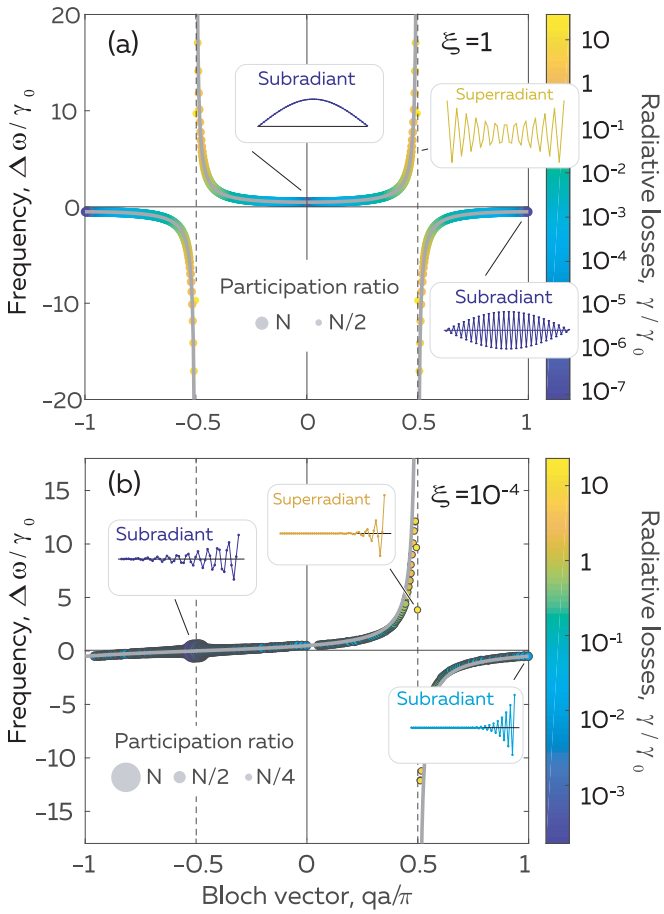

FIG. 7. (a) The resonant states of a symmetrically coupled ($\xi = 1$) array of $N = 400$ quantum emitters separated with $\varphi = \pi/2$. The dispersion of the infinite system is shown with a solid gray line. The color of labeling points denotes the normalized radiation loss rate for each state. The diameter of the labeling point corresponds to the normalized participation ratio. The typical R values are shown for eye guidance in the inset. Mode profiles in the insets are plotted for $N = 50$ for clearness. (b) The resonant states of the chirally coupled array with asymmetry parameter $\xi = 10^{-4}$. The parameters of computation are the same as in (a).

the emission rates of superradiant states $\gamma_{\mathrm{sup}} \propto N$ [11,63]. The radiative losses scaling law on N is shown in Fig. 8(a) for symmetric coupling $\xi = 1$. On the other hand, the effective distance to the edge of the array L_q also changes with ξ and gives its contribution to the modified radiation rate.

Since in the case of the ordered structure the eigenmodes of the system are constructed from the Bloch waves, the excitation occupies almost all of the lattice sites $R \sim N$. We have depicted the normalized participation ratio R/N for each mode in Fig. 7(a) with the diameter of the circle labeling the R value for each state. One can see that the superradiant states have the smallest R, while the subradiant states, in contrast, are the most extended ones with $R \approx N$. Moreover, all of the states in the ordered array scale linearly with the system size, so $R \propto N$, which is a sign of their truly extended nature. One also needs to mention a special case of $\varphi = 0$, which corresponds to a discrete Bardin-Cooper-Schrieffer model [64,65] and is proposed for the description of superconducting states

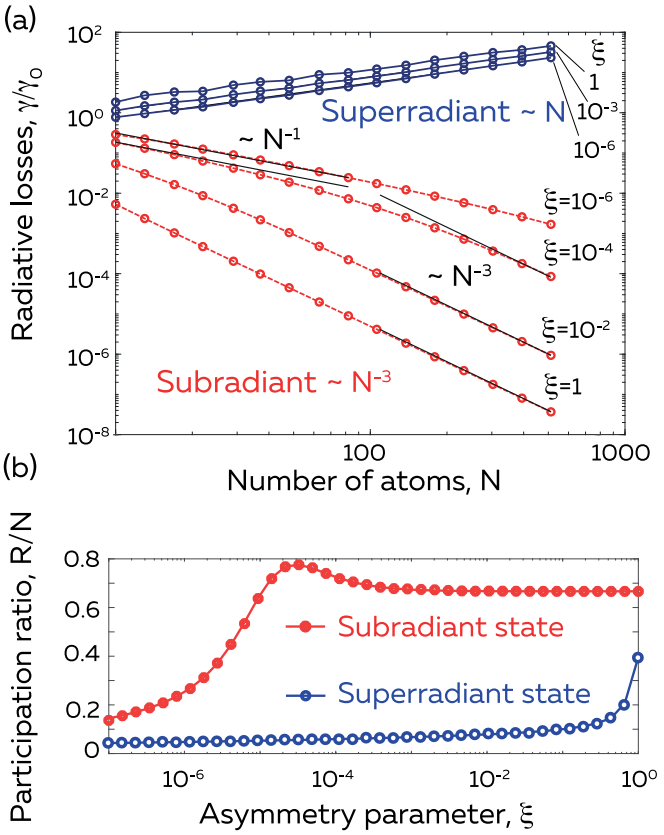

FIG. 8. (a) The radiative losses of the states with largest (superradiant) and smallest (subradiant) values of γ as a function of number of emitters for different values of asymmetry parameter ξ and $\varphi = \pi/2$. (b) The participation ratio of the corresponding super- and subradiant states as a function of asymmetry parameter for $N = 400$ and $\varphi = \pi/2$.

in lattice models. In this case, there appear $N-1$ degenerate states with zero radiative rate and one nondegenerate state, which has superradiant character with $\gamma_N = N\gamma_0$ and constant mode profile with in-phase amplitudes $|\psi\rangle = 1/\sqrt{N}\sum_n |n\rangle$.

2. Asymmetric coupling

Once the strongly asymmetric coupling is introduced for a finite system, discrete resonant states follow the dispersion behavior of an infinite structure as shown with a solid gray line in Fig. 7(b). One can see that the avoided crossing at $qa = -\varphi$ vanishes for asymmetric coupling, and the resonant states close to this point possess the lowest radiative losses. Interestingly, the radiative losses of subradiant states have different scaling with N comparing to a symmetric coupling case as one can see from Fig. 8(a), where the radiative losses are plotted in double logarithmic scale as functions of the emitter number N for various values of the asymmetry parameter ξ. It is worth noting that for small asymmetry parameter values the decay rate of subradiant states scales as $\gamma_{\text{sub}} \sim N^{-1}$ for $N \lesssim N^*$, while for larger $N \gtrsim N^*$ the scaling modifies to $\gamma_{\text{sub}} \sim N^{-3}$. As can be seen from Fig. 7(b), subradiant states appear close to the light line $qa = -\varphi$, where the band gap shrinks with the decrease of ξ as well as the region of the flat band, where the group velocity tends to zero. The switching between the linear dispersion regime and the flat band regime in the vicinity of the light line $qa = -\varphi$ provides the change in the radiative rate behavior. Indeed, the radiative decay rate of a state can be estimated as $\gamma(q) \sim v_g(q)/L_q$, where L_q is the characteristic distance from the mode center to the structure edge, and v_g is the group velocity. The group velocity rapidly changes in the vicinity of the light line from $v_g = q\gamma_0/4$ to $v_g \to 0$ as $|qa - \varphi| \sim 1\sqrt{\xi}$, which provides the observed change in the scaling of the radiative losses and gives the estimation for $N^* \approx 1/\sqrt{\xi}$.

The second factor which results in decrease of the radiative rate of chirally coupled systems compared to symmetric coupling is related to change of the R which also corresponds to characteristic length L_q, i.e., the smaller the value of R the faster the states escape through the edge by radiation. The dependence of the R on the asymmetry parameter is shown in Fig. 8(b). One can see that R for both sub- and superradiant states decreases with ξ, which increases the radiative rate for strongly asymmetric coupling.

Subradiant states have the largest R values close to N; therefore, the excitation occupies most of the array sites as shown by the label diameter in Fig. 7(b). However, now the modes become localized at the edge of the chain as it is shown in the insets of Fig. 7(b). If ξ becomes small enough, the excitation in the system is concentrated at the right side of the chain as has been discussed in the main text.

APPENDIX C: BASIC FORMULAS FOR TRANSFER MATRICES

The forward transmission coefficient $T_N \equiv |t_N^{\rightarrow}|^2$ in Eq. (7) can also be calculated numerically. This allows us to implement an independent calculation of the localization length, not relying on the evaluation of the eigenstates. To this end we use the transfer-matrix method. Starting from the relation between the fields to the left and right of the atom,

$$\begin{pmatrix} E_R^{\rightarrow} \\ E_R^{\leftarrow} \end{pmatrix} = M_{\text{atom}} \begin{pmatrix} E_L^{\rightarrow} \\ E_L^{\leftarrow} \end{pmatrix}, \tag{C1}$$

one can define the transfer matrix through a two-level atom M_{atom} [26]:

$$M_{\text{atom}} = \frac{1}{t_{\leftarrow}} \begin{pmatrix} t_{\rightarrow}t_{\leftarrow} - r^2 & r \\ -r & 1 \end{pmatrix} \tag{C2}$$

where r and $t_{\rightarrow}$ and $t_{\leftarrow}$ are reflection and forward and backward transmission coefficients of a single atom, respectively, given by [18]

$$r = \frac{i\sqrt{\gamma_L\gamma_R}}{\omega_0 - \omega - i\gamma_0/2},$$
$$t_{\rightarrow/\leftarrow} = 1 + \frac{i\gamma_{R/L}}{\omega_0 - \omega - i\gamma_0/2}. \tag{C3}$$

With the transfer matrix for a free part of the waveguide M_d being equal to

$$M_d = \begin{pmatrix} e^{i\omega d/c} & 0 \\ 0 & e^{-i\omega d/c} \end{pmatrix}, \tag{C4}$$

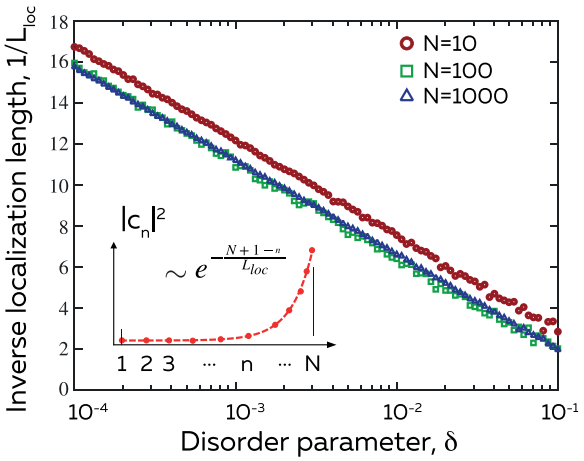

FIG. 9. Dimensionless inverse localization length $L_{\rm loc}^{-1}$ vs disorder parameter δ for different numbers of atoms in a chain of N unidirectionally coupled atoms $\xi = 0$. It has been extracted by fitting an exponential function to the probabilities of few atoms closest to the right edge of the chain being excited, as described by the inset.

we proceed to the total transfer matrix through an array of N atoms periodically placed with the distance d as follows:

$$M_N = (M_d M_{\rm atom})^N, \tag{C5}$$

and find reflection and transmission coefficients for the light incident from left as

$$r_N^{\leftarrow} = -\frac{[M_N]_{2,1}}{[M_N]_{2,2}}, \quad t_N^{\rightarrow} = \frac{\det M_N}{[M_N]_{2,2}}. \tag{C6}$$

APPENDIX D: DISORDER IN A PERFECTLY UNIDIRECTIONAL SYSTEM

The effective Hamiltonian for a regular 1D array of atoms that are unidirectionally coupled through a guided mode and experience a small disorder in transition frequencies can be formally expressed as

$$H_{\rm eff} = \begin{pmatrix} D_1 & 0 & 0 & \dots & 0 \\ ge^{i\phi} & D_2 & 0 & \dots & 0 \\ ge^{i2\phi} & ge^{i\phi} & D_3 & \dots & 0 \\ \dots & \dots & \dots & \dots & \dots \\ ge^{i(N-1)\phi} & ge^{i(N-2)\phi} & ge^{i(N-3)\phi} & \dots & D_N \end{pmatrix}, \tag{D1}$$

where $g = -i\hbar\gamma_0$, $D_k = \hbar(\Delta\omega_k - i\frac{\gamma_0}{2})$, and $\phi = k_0 d$. Owing to a disorder, the degeneracy of eigenstates, appearing as a result of interaction unidirectionality, is completely lifted. In this case we have a full set of eigenvectors $\mathbf{v^{(k)}}$ with the corresponding eigenvalues being equal to $\lambda_k = D_k$, and the latter simply comes from the $H_{\rm eff}$ matrix being a lower triangular one. One can explicitly find the jth component of eigenvector $\mathbf{v^{(k)}}$ to be equal to

$$v_j^{(k)} = A_k \Bigg(\delta_{j,N} + (1-\delta_{j,N}) H[j-k] \times \prod_{m=j+1}^{N} \frac{(D_k - D_m)}{(g + D_k - D_{m-1})} e^{-i(N-j)\phi} \Bigg), \tag{D2}$$

where A_k is the normalization constant and $H[j-k]$ is a discrete Heaviside function, being zero for $k > j$ and 1 otherwise. Even though the above formula is slightly cumbersome, it is much easier to understand if one considers the transformation matrix to the corresponding eigenspace $S = (\mathbf{v^{(1)}}, \mathbf{v^{(2)}}, \dots, \mathbf{v^{(N)}})$:

$$S = \begin{pmatrix} A_1 \frac{(D_1-D_2)\dots(D_1-D_N)e^{-i(N-1)\phi}}{(g+D_1-D_1)\dots(g+D_1-D_{N-1})} & 0 & \dots & 0 & 0 \\ A_1 \frac{(D_1-D_3)\dots(D_1-D_N)e^{-i(N-2)\phi}}{(g+D_1-D_2)\dots(g+D_1-D_{N-1})} & A_2 \frac{(D_2-D_3)\dots(D_2-D_N)e^{-i(N-2)\phi}}{(g+D_2-D_2)\dots(g+D_2-D_{N-1})} & \dots & 0 & 0 \\ \dots & \dots & \dots & \dots & \dots \\ A_1 \frac{(D_1-D_N)e^{-i\phi}}{(g+D_1-D_{N-1})} & A_2 \frac{(D_2-D_N)e^{-i\phi}}{(g+D_2-D_{N-1})} & \dots & A_{N-1}\frac{(D_{N-1}-D_N)e^{-i\phi}}{(g+D_{N-1}-D_{N-1})} & 0 \\ A_1 & A_2 & \dots & A_{N-1} & A_N \end{pmatrix}. \tag{D3}$$

As seen from the above, the matrix S is also lower triangular, and the Nth eigenstate corresponds to the last atom being excited solely, similarly to the case of absent disorder, which is a perfectly localized state with the corresponding participation ratio being $R(\mathbf{v^{(N)}}) = 1$. A simple inspection tells that, obviously, all other states $k \neq N$ have $R > 1$, but, simultaneously, even the state $\mathbf{v^{(1)}}$ with all nonzero components is not a delocalized one due to the fact that $\mathrm{var}(\Delta\omega_k) = \delta\gamma_0 \leqslant 0.1\gamma_0$ in our case. This is what is indicated in Fig. 9, where the dimensionless inverse localization length $L_{\rm loc}^{-1}$ (an effective number of excited atoms) is plotted against the disorder strength δ for different numbers of atoms in a chain. As seen, $L_{\rm loc}^{-1}$ monotonically decreases with the disorder δ following a logarithmical dependence almost perfectly. Moreover, even for the largest disorder parameter considered $\delta = 0.1$, $L_{\rm loc}^{-1} > 1$, which means that localization length is smaller than unity, hence we conclude that the most delocalized state in terms of R is, strictly speaking, a localized one. We can conclude that for a perfectly chiral case the introduction of disorder into atomic transition frequencies does not lead to localization-delocalization transition for the considered range of a disorder parameter δ.

[1] A. Lagendijk, B. Van Tiggelen, and D. S. Wiersma, Fifty years of Anderson localization, Phys. Today **62**(8), 24 (2009).

[2] P. W. Anderson, Absence of diffusion in certain random lattices, Phys. Rev. **109**, 1492 (1958).

[3] E. Abrahams, P. W. Anderson, D. C. Licciardello, and T. V. Ramakrishnan, Scaling Theory of Localization: Absence of Quantum Diffusion in Two Dimensions, Phys. Rev. Lett. **42**, 673 (1979).

[4] N. Hatano and D. R. Nelson, Localization Transitions in Non-Hermitian Quantum Mechanics, Phys. Rev. Lett. **77**, 570 (1996).

[5] P. W. Brouwer, P. G. Silvestrov, and C. W. J. Beenakker, Theory of directed localization in one dimension, Phys. Rev. B **56**, R4333(R) (1997).

[6] P. W. Brouwer, C. Mudry, B. D. Simons, and A. Altland, Delocalization in Coupled One-Dimensional Chains, Phys. Rev. Lett. **81**, 862 (1998).

[7] F. Hébert, M. Schram, R. T. Scalettar, W. B. Chen, and Z. Bai, Hatano-Nelson model with a periodic potential, Eur. Phys. J. B **79**, 465 (2011).

[8] J. Feinberg and A. Zee, Non-Hermitian localization and delocalization, Phys. Rev. E **59**, 6433 (1999).

[9] D. E. Chang, J. S. Douglas, A. González-Tudela, C. L. Hung, and H. J. Kimble, Colloquium: Quantum matter built from nanoscopic lattices of atoms and photons, Rev. Mod. Phys. **90**, 031002 (2018).

[10] A. S. Sheremet, M. I. Petrov, I. V. Iorsh, A. V. Poshakinskiy, and A. N. Poddubny, Waveguide quantum electrodynamics: collective radiance and photon-photon correlations, arXiv:2103.06824.

[11] H. R. Haakh, S. Faez, and V. Sandoghdar, Polaritonic normal-mode splitting and light localization in a one-dimensional nanoguide, Phys. Rev. A **94**, 053840 (2016).

[12] A. V. Poshakinskiy, J. Zhong, and A. N. Poddubny, Quantum Chaos Driven by Long-Range Waveguide-Mediated Interactions, Phys. Rev. Lett. **126**, 203602 (2021).

[13] N. Fayard, L. Henriet, A. Asenjo-Garcia, and D. E. Chang, Many-body localization in waveguide quantum electrodynamics, Phys. Rev. Res. **3**, 033233 (2021).

[14] G. Malpuech and A. Kavokin, Absorption of light by inhomogeneously broadened excitons in quantum wells, Semicond. Sci. Technol. **14**, 1031 (1999).

[15] V. A. Kosobukin, Exciton polaritons and their one-dimensional localization in disordered quantum-well structures, Phys. Solid State **45**, 1145 (2003).

[16] V. A. Kosobukin and A. N. Poddubny, Exciton-polariton absorption in periodic and disordered quantum-well chains, Phys. Solid State **49**, 1977 (2007).

[17] A. Lubatsch and J. Kroha, Optically driven Mott-Hubbard systems out of thermodynamic equilibrium, Ann. Phys. (Leipzig) **521**, 863 (2010).

[18] P. Lodahl, S. Mahmoodian, S. Stobbe, A. Rauschenbeutel, P. Schneeweiss, J. Volz, H. Pichler, and P. Zoller, Chiral quantum optics, Nature (London) **541**, 473 (2017).

[19] I. M. Mirza, J. G. Hoskins, and J. C. Schotland, Chirality, band structure, and localization in waveguide quantum electrodynamics, Phys. Rev. A **96**, 053804 (2017).

[20] I. M. Mirza and J. C. Schotland, Influence of disorder on electromagnetically induced transparency in chiral waveguide quantum electrodynamics, J. Opt. Soc. Am. B **35**, 1149 (2018).

[21] H. H. Jen, Disorder-assisted excitation localization in chirally coupled quantum emitters, Phys. Rev. A **102**, 043525 (2020).

[22] N. Okuma, K. Kawabata, K. Shiozaki, and M. Sato, Topological Origin of Non-Hermitian Skin Effects, Phys. Rev. Lett. **124**, 086801 (2020).

[23] E. J. Bergholtz, J. C. Budich, and F. K. Kunst, Exceptional topology of non-hermitian systems, Rev. Mod. Phys. **93**, 015005 (2021).

[24] N. Okuma and M. Sato, Non-Hermitian topological phenomena: A review, arXiv:2205.10379.

[25] K. Kawabata and S. Ryu, Nonunitary Scaling Theory of Non-Hermitian Localization, Phys. Rev. Lett. **126**, 166801 (2021).

[26] N. V. Corzo, B. Gouraud, A. Chandra, A. Goban, A. S. Sheremet, D. V. Kupriyanov, and J. Laurat, Large Bragg Reflection from One-Dimensional Chains of Trapped Atoms Near a Nanoscale Waveguide, Phys. Rev. Lett. **117**, 133603 (2016).

[27] L. Lu, J. D. Joannopoulos, and M. Soljačić, Topological photonics, Nat. Photonics **8**, 821 (2014).

[28] S. Barik, A. Karasahin, S. Mittal, E. Waks, and M. Hafezi, Chiral quantum optics using a topological resonator, Phys. Rev. B **101**, 205303 (2020).

[29] M. Jalali Mehrabad, A. P. Foster, R. Dost, A. M. Fox, M. S. Skolnick, and L. R. Wilson, Chiral topological photonics with an embedded quantum emitter, Optica **7**, 1690 (2020).

[30] M. Jalali Mehrabad, A. P. Foster, R. Dost, E. Clarke, P. K. Patil, I. Farrer, J. Heffernan, M. S. Skolnick, and L. R. Wilson, A semiconductor topological photonic ring resonator, Appl. Phys. Lett. **116**, 061102 (2020).

[31] A. Asenjo-Garcia, J. D. Hood, D. E. Chang, and H. J. Kimble, Atom-light interactions in quasi-one-dimensional nanostructures: A Green's-function perspective, Phys. Rev. A **95**, 033818 (2017).

[32] K. P. Nayak, M. Sadgrove, R. Yalla, F. Le Kien, and K. Hakuta, Nanofiber quantum photonics, J. Opt. **20**, 073001 (2018).

[33] I. S. Besedin, M. A. Gorlach, N. N. Abramov, I. Tsitsilin, I. N. Moskalenko, A. A. Dobronosova, D. O. Moskalev, A. R. Matanin, N. S. Smirnov, I. A. Rodionov, A. N. Poddubny, and A. V. Ustinov, Topological excitations and bound photon pairs in a superconducting quantum metamaterial, Phys. Rev. B **103**, 224520 (2021).

[34] T. Gruner and D.-G. Welsch, Green-function approach to the radiation-field quantization for homogeneous and inhomogeneous Kramers-Kronig dielectrics, Phys. Rev. A **53**, 1818 (1996).

[35] E. Ivchenko, A. Nesvizhskii, and S. Jorda, Resonant Bragg reflection from quantum-well structures, Superlattices Microstruct. **16**, 17 (1994).

[36] M. R. Vladimirova, E. L. Ivchenko, and A. V. Kavokin, Exciton polaritons in long-period quantum-well structures, Semiconductors **32**, 90 (1998).

[37] G. Angelatos and S. Hughes, Polariton waveguides from a quantum dot chain in a photonic crystal waveguide: An architecture for waveguide quantum electrodynamics, Optica **3**, 370 (2016).

[38] D. F. Kornovan, A. S. Sheremet, and M. I. Petrov, Collective polaritonic modes in an array of two-level quantum emitters coupled to optical nanofiber, Phys. Rev. B **94**, 245416 (2016).

[39] I. M. Lifshitz, S. A. Gredeskul, and L. A. Pastur, *Introduction to the Theory of Disordered Systems* (Wiley, New York, 1988).

[40] A. N. Poddubny, M. V. Rybin, M. F. Limonov, and Y. S. Kivshar, Fano interference governs wave transport in disordered systems, Nat. Commun. **3**, 914 (2012).

[41] B. A. Van Tiggelen, Localization of Waves, in *Diffuse Waves in Complex Media*, edited by J.-P. Fouque (Springer Netherlands, Dordrecht, 1999), pp. 1–60.

[42] P. Biswas, P. Cain, R. A. Römer, and M. Schreiber, Off-diagonal disorder in the Anderson model of localization, Phys. Status Solidi B **218**, 205 (2000).

[43] F. Dyson, The dynamics of a disordered linear chain, Phys. Rev. **92**, 1331 (1953).

[44] G. G. Kozlov, V. A. Malyshev, F. Domínguez-Adame, and A. Rodríguez, Zero-energy peak of the density of states and localization properties of a one-dimensional Frenkel exciton: Off-diagonal disorder, Phys. Rev. B **58**, 5367 (1998).

[45] M. Petrov, Disorder-induced Purcell enhancement in nanoparticle chains, Phys. Rev. A **91**, 023821 (2015).

[46] A. Croy, P. Cain, and M. Schreiber, Anderson localization in 1D systems with correlated disorder, Eur. Phys. J. B **82**, 107 (2011).

[47] R. Mitsch, C. Sayrin, B. Albrecht, P. Schneeweiss, and A. Rauschenbeutel, Quantum state-controlled directional spontaneous emission of photons into a nanophotonic waveguide, Nat. Commun. **5**, 5713 (2014).

[48] P. O. Guimond, B. Vermersch, M. L. Juan, A. Sharafiev, G. Kirchmair, and P. Zoller, A unidirectional on-chip photonic interface for superconducting circuits, npj Quantum Inf. **6**, 32 (2020).

[49] E. Vetsch, D. Reitz, G. Sague, R. Schmidt, S. T. Dawkins, and A. Rauschenbeutel, Optical Interface Created by Laser-Cooled Atoms Trapped in the Evanescent Field Surrounding an Optical Nanofiber, Phys. Rev. Lett. **104**, 203603 (2010).

[50] B. Vermersch, T. Ramos, P. Hauke, and P. Zoller, Implementation of chiral quantum optics with Rydberg and trapped-ion setups, Phys. Rev. A **93**, 063830 (2016).

[51] A. N. Poddubny, Quasiflat band enabling subradiant two-photon bound states, Phys. Rev. A **101**, 043845 (2020).

[52] S. Mahmoodian, M. Čepulkovskis, S. Das, P. Lodahl, K. Hammerer, and A. S. Sørensen, Strongly Correlated Photon Transport in Waveguide Quantum Electrodynamics with Weakly Coupled Emitters, Phys. Rev. Lett. **121**, 143601 (2018).

[53] S. Mahmoodian, G. Calajó, D. E. Chang, K. Hammerer, and A. S. Sørensen, Dynamics of Many-Body Photon Bound States in Chiral Waveguide QED, Phys. Rev. X **10**, 031011 (2020).

[54] A. S. Prasad, J. Hinney, S. Mahmoodian, K. Hammerer, S. Rind, P. Schneeweiss, A. S. Sørensen, J. Volz, and A. Rauschenbeutel, Correlating photons using the collective nonlinear response of atoms weakly coupled to an optical mode, Nat. Photonics **14**, 719 (2020).

[55] R. Frank, Coherent control of Floquet-mode dressed plasmon polaritons, Phys. Rev. B **85**, 195463 (2012).

[56] A. Lubatsch and R. Frank, Evolution of Floquet topological quantum states in driven semiconductors, Eur. Phys. J. B **92**, 215 (2019).

[57] A. Lubatsch and R. Frank, Behavior of Floquet topological quantum states in optically driven semiconductors, Symmetry **11**, 1246 (2019).

[58] B. Bakkensen, Y.-X. Zhang, J. Bjerlin, and A. S. Sørensen, Photonic bound states and scattering resonances in waveguide QED, arXiv:2110.06093.

[59] M. Voronov, E. Ivchenko, M. Erementchouk, L. Deych, and A. Lisyansky, Photoluminescence spectroscopy of one-dimensional resonant photonic crystals, J. Lumin. **125**, 112 (2007).

[60] R. Movassagh and L. P. Kadanoff, Eigenpairs of Toeplitz and disordered Toeplitz matrices with a Fisher-Hartwig symbol, J. Stat. Phys. **167**, 959 (2017).

[61] A. Asenjo-Garcia, M. Moreno-Cardoner, A. Albrecht, H. J. Kimble, and D. E. Chang, Exponential Improvement in Photon Storage Fidelities Using Subradiance and "Selective Radiance" in Atomic Arrays, Phys. Rev. X **7**, 031024 (2017).

[62] Y.-X. Zhang, C. Yu, and K. Mølmer, Subradiant bound dimer excited states of emitter chains coupled to a one dimensional waveguide, Phys. Rev. Res. **2**, 013173 (2020).

[63] R. H. Dicke, Coherence in spontaneous radiation processes, Phys. Rev. **93**, 99 (1954).

[64] R. Modak, S. Mukerjee, E. A. Yuzbashyan, and B. S. Shastry, Integrals of motion for one-dimensional Anderson localized systems, New J. Phys. **18**, 033010 (2016).

[65] G. L. Celardo, R. Kaiser, and F. Borgonovi, Shielding and localization in the presence of long-range hopping, Phys. Rev. B **94**, 144206 (2016).